



ORIGINAL ARTICLE

Copper doped manganese dioxide as counter electrode for dye-sensitized solar cells



Belqasem Aljafari^{a,*,1}, Subbiah Vijaya^{b,1}, Arash Takshi^{c,d}, Sambandam Anandan^b

^a Department of Electrical Engineering, College of Engineering, Najran University, Najran 11001, Saudi Arabia

^b Nanomaterials & Solar Energy Conversion Lab, Department of Chemistry, National Institute of Technology, Tiruchirappalli 620015, India

^c Department of Electrical Engineering, University of South Florida, 4202 E Fowler Ave, Tampa, FL 33620, USA

^d Clean Energy Research Center, University of South Florida, 4202 E Fowler Ave, Tampa, FL 33620, USA

Received 18 April 2022; accepted 20 June 2022

Available online 24 June 2022

KEYWORDS

Cu doped MnO₂;
Counter electrode;
DSSC;
Efficiency;
IPCE

Abstract Many materials have been tried as the counter electrode (CE) material as a substitute to the noble metal Pt in dye-sensitized solar cells (DSSCs). The CE property is critical to the operation of a DSSC as it catalyzes the reduction of I₃⁻ ions and retrieves the electrons from the photoanode. Here we have explored the application of manganese dioxide (MnO₂) and copper-doped manganese dioxide (Cu-MnO₂) nanoparticles as CE candidates for DSSCs mainly as low-cost alternatives to Pt. A simple hydrothermal method was followed to synthesize α-MnO₂ and Cu-MnO₂ nanoparticles at a temperature of 140 °C for 14 h. The nanoparticles were characterized to prove its electrocatalytic abilities for DSSCs. DSSC devices fabricated with 10 wt% Cu-MnO₂ as CE showed the best V_{OC} of 781 mV, I_{SC} of 3.69 mA/cm², FF of 0.50, and %PCE of 1.7 whereas Pt as CE showed V_{OC} of 780 mV, I_{SC} of 14.8 mA/cm², FF of 0.43, and %PCE of 5.83 under **0.85 Sun**. The low-cost feature of using Cu-MnO₂ is encouraging to further study the factors that can improve the efficiency of DSSCs with alternative CEs to conventional Pt electrodes.

© 2022 The Author(s). Published by Elsevier B.V. on behalf of King Saud University. This is an open access article under the CC BY-NC-ND license (<http://creativecommons.org/licenses/by-nc-nd/4.0/>).

1. Introduction

Photovoltaic is truly a sustainable and environmentally friendly method of producing energy [Kiran et al., 2016; Zulkifli et al., 2015]. Dye-sensitized solar cells (DSSCs) are alternatives to silicon solar cells with the advantages of higher efficiency in diffused light, better cost-effectiveness, and easy fabrication [Chiba et al., 2006]. DSSC has four major parts: photoanode, sensitizer, redox electrolyte, and photocathode. The typical choice of photocathode or counter electrode (CE) material is platinum (Pt) due to its high catalytic activity and excellent stability toward the iodide redox species [Kim et al., 2006]. Since it is a costly noble metal and retreating supply, other materials have been under search to substitute Pt [Thomas et al., 2014]. Conducting poly-

* Corresponding author.

E-mail addresses: bhaljafari@nu.edu.sa (B. Aljafari), sanand@nitt.edu (S. Anandan).

¹ Equally Contribute.

Peer review under responsibility of King Saud University.



Production and hosting by Elsevier

mers, carbonaceous materials, and transition metal compounds are some of the alternative materials introduced for the fabrication of DSSCs [Thomas et al., 2014].

It should have an energy level that matches the electrolyte potential and possess enhanced electrocatalytic activity, good reflectivity, and high surface area. Besides transparency, good reflectivity of CE is needed for illumination on the photoanode side. The electrochemically active surface of the CE should also preferentially be porous, have an optimum thickness, have chemical and electrochemical stability, be resistant to corrosion, have good adhesivity with the substrate, be low-cost, and be environmentally friendly. Atli and Yildiz (2022) reported a power conversion efficiency of 5.06% even with opaque Pt film assigned as a CE compared to transparent Pt CE (4.31%). This is because the high coverage (homogeneity) occurs in the case of transparent Pt CE due to the smaller particle size leading to an increase in the possibility of light interactions and reflections. [Atli and Yildiz, 2021; Atilgan and Yildiz, 2022].

Noticed, wide studies have been reported towards conducting polymers (poly(3,4-propylenedioxythiophene), polypyrrole (PPy), porous poly(3,4-propylenedioxythiophene), polythiophene (PTs), etc.) as cathodes in DSSCs due to their good conductivity, and environmental stability [Jeon et al., 2011; Huang et al., 2012; Kim et al., 2011]. Likewise, carbon families (activated carbon, carbon nanotubes, and graphene) show exceptional catalytic activity towards the redox species upon being used as CEs in DSSCs [Murakami et al., 2008; Nam et al., 2010].

Transition metal carbides (MoC, VC, WC, NbC, TiC, Cr₃C₂, and Ta₄C₃) may act as smart CE materials because of superior catalytic activity, high electrical conductivity, and good thermal stability properties [Wu et al., 2012; Yun et al., 2013; Paranthaman et al., 2016]. Cai et al., 2017 fabricated DSSCs using copper-doped iron carbide (0.75%) as CEs resulting in the highest energy conversion efficiency of 5.68%. Such efficiency may be due to the excellent conductive properties of uniformly dispersed copper over iron carbide, which facilitates high electron transfer. Noble metal-like behavior of transition metal nitrides (TiN, MoN, WN, VN, NbN, CrN, NiN, Mo₂N, W₂N, Fe₂N, and Ta₄N₅) due to the electronic structure similarity renders them as CE materials in DSSCs [Furimsky 2003; Kang et al., 2015; Zhang et al., 2012; Jiang et al., 2009]. Also, metal chalcogenides of various compositions were introduced as CEs show enhanced photovoltaic performance than ubiquitous platinumized cathodes [Olsen et al., 2000]. Wu et al. fabricated DSSCs with MoS₂ and WS₂ as CEs that results in photoconversion efficiency of 7.59 % and 7.73 %, respectively [Wu et al., 2011]. Yildiz et al. reported Iron Phosphide (FeP) as CEs generates an efficiency of 3.96% which is comparable to the Pt CE. Besides, DSSCs are fabricated with transition metal oxides such as WO₂ and NbO₂ as CE generates photoconversion efficiency of 7.25% and 7.88% found close to DSSC with Pt CE (7.57%) [Zhou et al., 2013; Lin et al., 2011]. Ahmad et al., 2017 have synthesized α -MnO₂ nanorods by facile hydrothermal method and utilized them as CE in DSSCs resulting in an open-circuit voltage of 0.75 V and fill factor (0.38). Likewise, MnO₂-coated carbon nanofiber was used as CE which resulted in higher open-circuit voltage (0.78 V), fill factor (0.68), and PCE (8.86%). In continuation, various researchers coupled MnO₂ with NiO and TiO₂ layer-by-layer architecture and utilized them as CEs for DSSCs which shows higher efficiency compared to the pristine MnO₂ layer [Kakroo et al. 2020, Datta et al. 2020]. Copper having excellent conductive properties upon doped on MnO₂ results in enhanced electrochemical behaviour [Li et al., 2013; Ding 2010; Davis et al., 2014; Gao et al., 2018; Julien et al., 2017; Wei et al., 2011; Kakroo et al., 2020]. Considering the various choices of materials, the search for finding a low-resistance and low-cost alternative to Pt still needs more research [Thomas et al., 2014]. The promising results from doped metal oxides have motivated us to further study MnO₂ and Cu doped MnO₂ as CEs in DSSCs, particularly focusing on the effect of doping level on the performance of the MnO₂ electrode as a CE for DSSCs. This is because the transition metal oxide MnO₂ has certain advantages such as low-cost, high natural abundance, high

theoretical capacity (1370 Fg⁻¹), high voltage window, etc. Since its capacitance and conductivity are low, cationic doping has been proved to be effective to improve the conductivity and of which copper cations are found to improve electrochemical performance far better compared to other cations [An et al. 2019]. Further, the conductivity is based on electron concentration and mobility of electrons and hence we preferred to choose low dopant ratios (1, 5, 10 %wt). Hence in this study, MnO₂ and copper doped MnO₂ nanoparticles were prepared by hydrothermal approach and investigated as CEs in DSSCs.

2. Experimental methods

135 ml deionized water (DI) was added to potassium permanganate (KMnO₄) (1185.25 mg) slowly as the solution was stirred until it was dissolved completely. Then, different weight percentages (1, 5, 10 %) of copper acetate were added until it was fully dissolved. Afterward, the mixture was acidified by adding 2.5 ml of HCl. The whole mixture was transferred to a Teflon-lined autoclave and kept at 140 °C for 14 h. Finally, the product (Cu doped MnO₂) was regenerated by washing with DI water, and ethanol and dried at 80 °C for 24 hrs. A similar procedure was followed in the absence of copper acetate to generate pristine MnO₂ [Luo et al., 2008].

Refer to supporting information regarding a list of equipment used to characterize the prepared nanomaterials and for the experimental procedure followed towards the fabrication of solar cell devices.

3. Results and discussions

As shown in Fig. 1(A), the XRD pattern of the synthesized pristine MnO₂ and 1, 5, & 10 wt% copper doped MnO₂ nanoparticles by the hydrothermal method exhibited a well-defined diffraction pattern which is in good harmony with the testified crystalline α -MnO₂ (JCPDS data card no. 44-0141). [Ahmad et al., 2017; Yang et al., 2019] The diffraction peaks of both the samples appear at (12.6°), (18.03°), (28.5°), (37.4°), (41.5°), (49.8°), (55.9°), (59.8°), and (65.3°), are corresponding to the (110), (200), (310), (211), (301), (411), (600), (521), and (002) planes of α -MnO₂ respectively [Ahmad et al., 2017]. XRD patterns of Cu doped MnO₂ samples were also studied and results without any alterations in peaks belonging to α -MnO₂ were observed. Since the copper species are highly homogeneous and well dispersed; hence no characteristic peak of Cu or CuO has been seen even for the 10 wt% Cu doped MnO₂ sample [Yang et al., 2019]. The calculated crystallite size (using Scherrer formula) of 10 wt% Cu doped MnO₂ is found smaller (23 nm) compared to the pristine MnO₂ sample (27 nm).

Similar to XRD, both MnO₂ and 1, 5, & 10 wt% Cu doped MnO₂ show the same IR stretching peaks upon the analysis in the Fourier Transform-Infrared (FTIR) spectrometer (Fig. 1 (B)). The stretching and bending vibrations of the hydroxyl groups and the hydrogen-bonded surface water molecules are found at 3438 cm⁻¹ and 1629 cm⁻¹ [Yang et al., 2019; Mondal et al., 2018; Mondal et al., 2019] The Mn-O vibration band is seen near 700 cm⁻¹ which further supports the formation of MnO₂. Such observed results are due to two factors: (i) the amount of doping is a trace (even increased to 10%) and (ii) due to the same crystal size Cu doping can substitute manganese ions (results peak broadening). [Mondal et al., 2018].

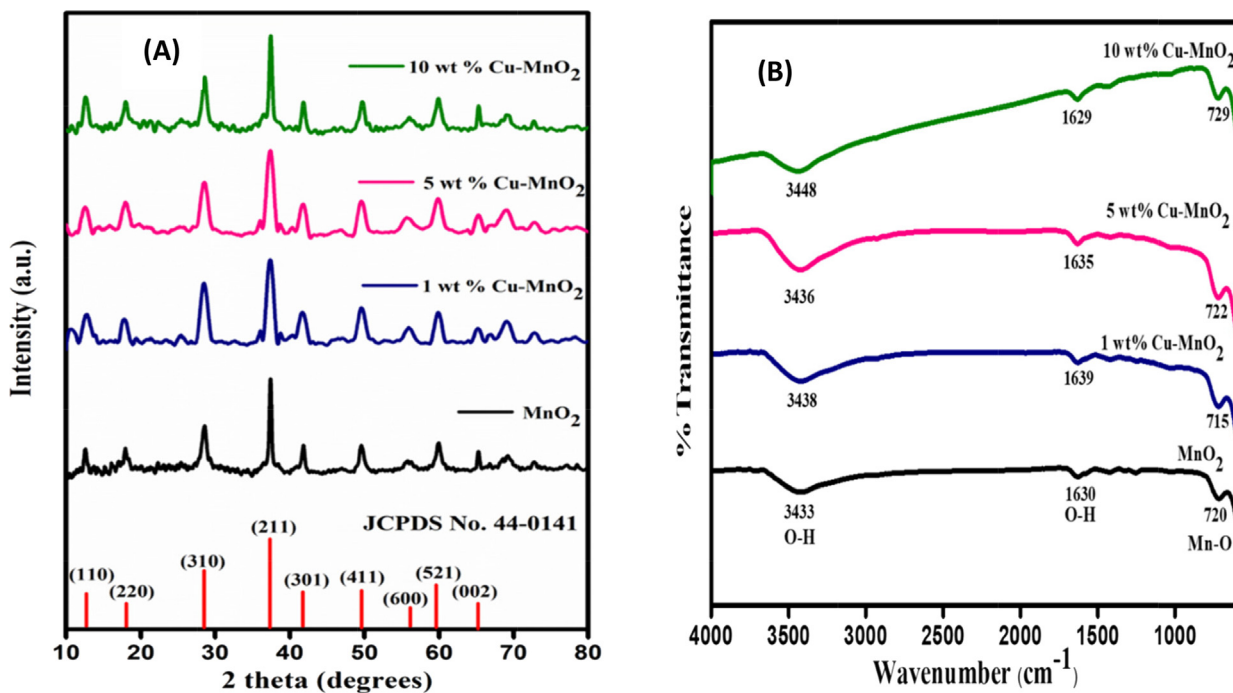


Fig. 1 (A) XRD patterns and (B) FTIR spectra of MnO₂ and 1, 5, & 10 wt% Cu doped MnO₂ nanoparticles.

To determine the optical energy bandgap of MnO₂ and Cu doped MnO₂ nanoparticles, the UV-Vis absorption spectrum was recorded. All the samples show a broad absorption band starting from 800 nm onwards which can be recognized due to d-d transitions of manganese ions (Figure not provided). The photoexcited electron from the valence band to the conduction band takes place due to Mn 3d energy level splitting [Mondal et al., 2018; Mondal et al., 2019]. Converting the photoabsorption data to the Tauc plots in Fig. 2, the optical energy bandgap (E_g) was predicted indirectly from the plots by using the following formula:

$$E_g = \frac{1240}{\text{Wavelength}}$$

Pristine MnO₂ shows a bandgap value of about 1.67 eV and upon doping with copper (1, 5, 10 wt%) noticed bandgap get lowers to 1.6, 1.49, and 1.43 eV which clearly illustrates that light absorption got enhanced with Cu dopant (Fig. 2). In addition, such copper dopants may suppress the recombination rates at the electrode/electrolyte/dye interfaces [Atilgan and Yildiz, 2022].

Both pure MnO₂ and Cu doped MnO₂ looked semispherical with coarse surface morphology under FE-SEM analysis (Fig. 3 a-d). Compared with pristine MnO₂, Cu doped MnO₂ has a slight difference in morphology and not noticed any lump which proved no agglomeration of particles. Such a larger particle size increases the scattering of light and thus allows the way light travels inside the device [Atli and Yildiz, 2022; Atilgan and Yildiz, 2022]. Besides it favors the penetration of the electrolyte and hence occurs quick electron transfer between the mediators (iodide/triiodide) in the electrolyte and the CE [Yang et al., 2019; Vijayakumar et al., 2015]. The EDX elemental analysis confirms the existence of individual metals only in the prepared pure MnO₂ (Mn-67.21; O-32.78) and 10 wt% Cu doped MnO₂ (Cu-9.12; Mn-55.22; O-

35.66) samples (Fig. 3 e,f). It is found that the observed EDX results are almost matching with the 10 wt% Copper dopant amount taken for the experiment. In TEM analysis (Fig. 3 g,h,j,k), also, samples show similar spherical morphology as seen in the SEM images. The selected area electron diffraction patterns also illustrate the samples were well crystallized in nature. (Fig. 3 i,l).

The cyclic voltammograms (CVs) of MnO₂ and copper doped MnO₂ thin layer electrodes (Fig. 4) look sigmoidal and symmetrical in shape due to the slow ion transport that may stimulate the fabricated DSSCs towards the effect of sunlight and as well as avoid back electron transfer. As can be observed from CV loops, the device having the Pt shows the highest I_{PC} and E_{PP} value (4.80 mAcm⁻² and 1000 mV) which indirectly indicates the good electrocatalytic activity of Pt CEs toward the liquid electrolyte [Yildiz et al. 2021]. Again, the higher I_{PC} suggests a better electrocatalytic activity which may be reflected in the device's performance. No certain oxidation and reduction peaks for Cu doped MnO₂ samples, hence it is not possible to determine I_{PC} and E_{PP} values. Since the prepared Pt-coated electrode showed a symmetric response with the two distinct peaks due to fast electron transfer from the counter electrode to the electrolyte (reduction of iodine/iodide electrolyte: $I_3 + 2e^- \rightarrow 3I^-$) [Vijaya et al., 2021].

Cu doped MnO₂ coated FTO glass plates were sandwiched one above the other for symmetrical dummy cell fabrication towards electrochemical impedance spectroscopy (EIS) measurements. Parafilm was used to avoid contact with each other. The electrolyte (an iodide/triiodide (I^-/I_3^-) solution) consisting of LiI/I₂ (0.05 M/0.01 M), and LiClO₄ (0.5 M) dissolved in 3-methoxy-propionitrile was injected in between the two glass plates. The electrochemical impedance spectroscopy (EIS) studies for such thin layer symmetrical electrodes were carried out under the following experimental conditions (frequency – 0.1 to 10⁵ Hz; AC voltage – 10 mV). The Nyquist plot (Fig. 5)

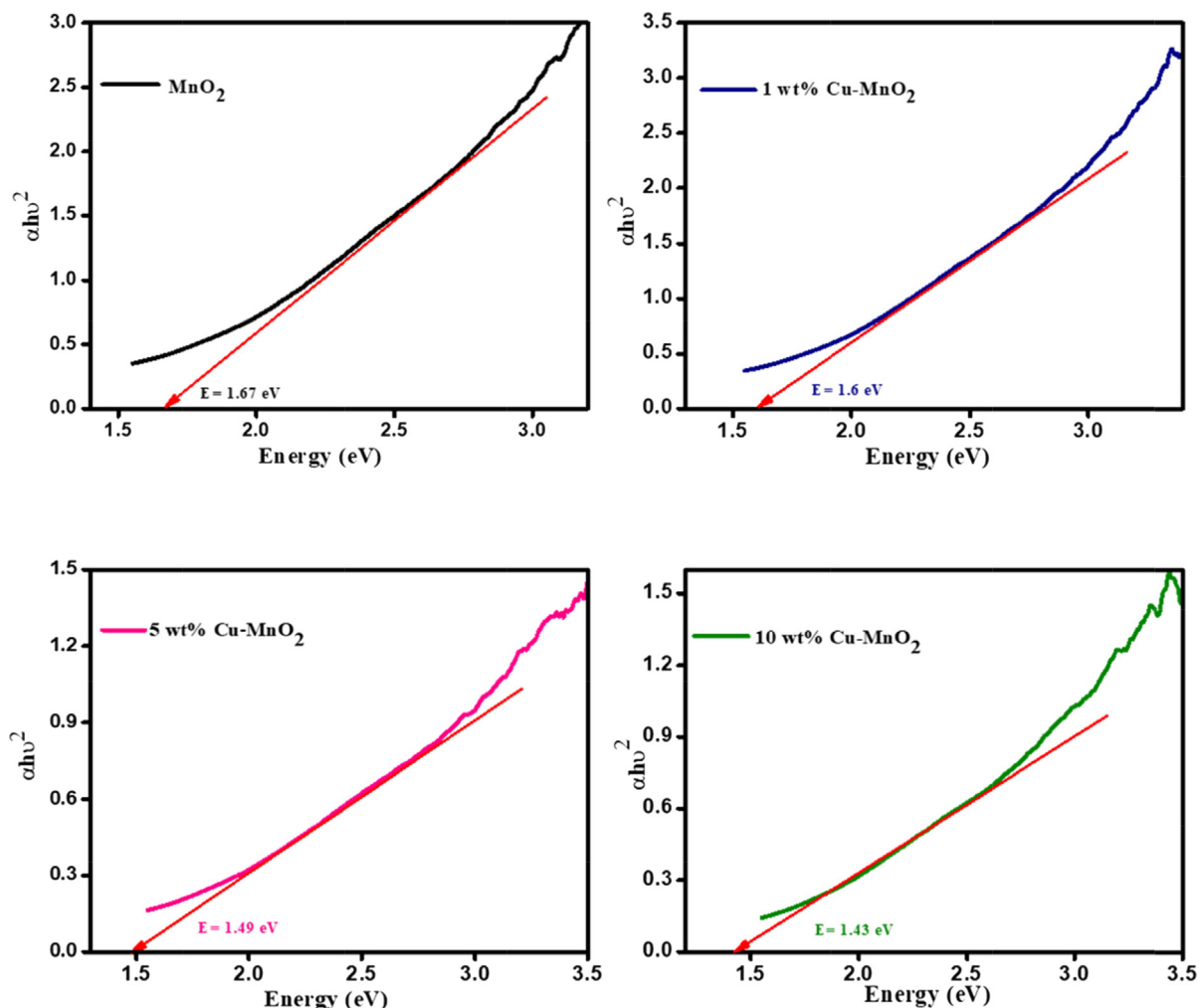


Fig. 2 Tauc plot of MnO_2 and 1, 5, & 10 wt% Cu doped MnO_2 nanoparticles.

is projected against real impedance (Z') vs imaginary impedance ($-Z''$) gives information about the resistance data at $\text{TiO}_2/\text{dye}/\text{electrolyte}$ and $\text{electrolyte}/\text{CE}$. Also included equivalent circuit model in the inset of Fig. 5. The electron-hole charge transfer, diffusion of ions, and electron recombination at the $\text{TiO}_2/\text{dye}/\text{electrolyte}$ interface are related to resistance. The series/bulk resistance (R_S) represents the FTO plates resistance along with the resistance of the counter electrodes can be investigated from the origin of the semicircle (the high-frequency region). The diameter of the semicircle of the mid-frequency region represents the charge transfer resistance (R_{CT}) indicates the I^-/I_3^- reduction catalytic activity [Wu et al. 2017]. The response at low frequency region is attributed to Warburg resistance, Z_w of I_3^- , tri-iodide diffusion [Wang et al. (2015)]. Further, the EIS parameters extracted from the Nyquist plot (Fig. 5) are listed in Table 1. From this table, the R_S values of the respective CEs follow the order: 1 wt% Cu- MnO_2 CE ($38.62 \Omega \text{ cm}^2$) > 10 wt% Cu- MnO_2 CE ($35.55 \Omega \text{ cm}^2$) > Pt CE ($31.97 \Omega \text{ cm}^2$) > MnO_2 CE ($30.29 \Omega \text{ cm}^2$) > 5 wt% Cu- MnO_2 CE ($29.87 \Omega \text{ cm}^2$). The R_S values of the Pt ($31.97 \Omega \text{ cm}^2$) is less than 10 wt% Cu doped MnO_2 ($35.55 \Omega \text{ cm}^2$) confirming the superior electrical conductivity of the Pt electrode. Further, the 1 wt% Cu doped MnO_2 shows the lowest R_{CT} value of $157.95 \Omega \text{ cm}^2$ compared

to Pt ($191.53 \Omega \text{ cm}^2$) and 10 wt% Cu doped MnO_2 ($204.9 \Omega \text{ cm}^2$). The better electrocatalytic activity of Cu doped MnO_2 toward the liquid iodide/triiodide electrolyte is confirmed by these EIS results.

Also, Bode phase plots for thin layer electrodes were measured to calculate the electron lifetimes (Fig. 6) from the equation.

$$\tau = \frac{1}{2\pi f}$$

where τ - electron lifetime and f - frequency [Sarker et al., 2014]. The calculated electron lifetime for Pt, MnO_2 , 1 wt% Cu- MnO_2 , 5 wt% Cu- MnO_2 , and 10 wt% Cu- MnO_2 CEs dummy cells are found to be 99, 32, 43, 57, and 75 ms. The peak noticed in the high-frequency region is correlated to the charge transfer that occurs at the electrode/electrolyte interfaces [Kim et al., 2012]. Copper-doped MnO_2 samples are found to have a phase shift lower than undoped samples indicating lower resistance for pristine MnO_2 samples.

To determine exchange current density (current at zero overpotential), Tafel polarization experiments were conducted for thin layer electrodes. Tafel polarization of the dummy cells has been plotted to further analyze the electrocatalytic behaviour of CEs. For that, dummy cells have been fabricated

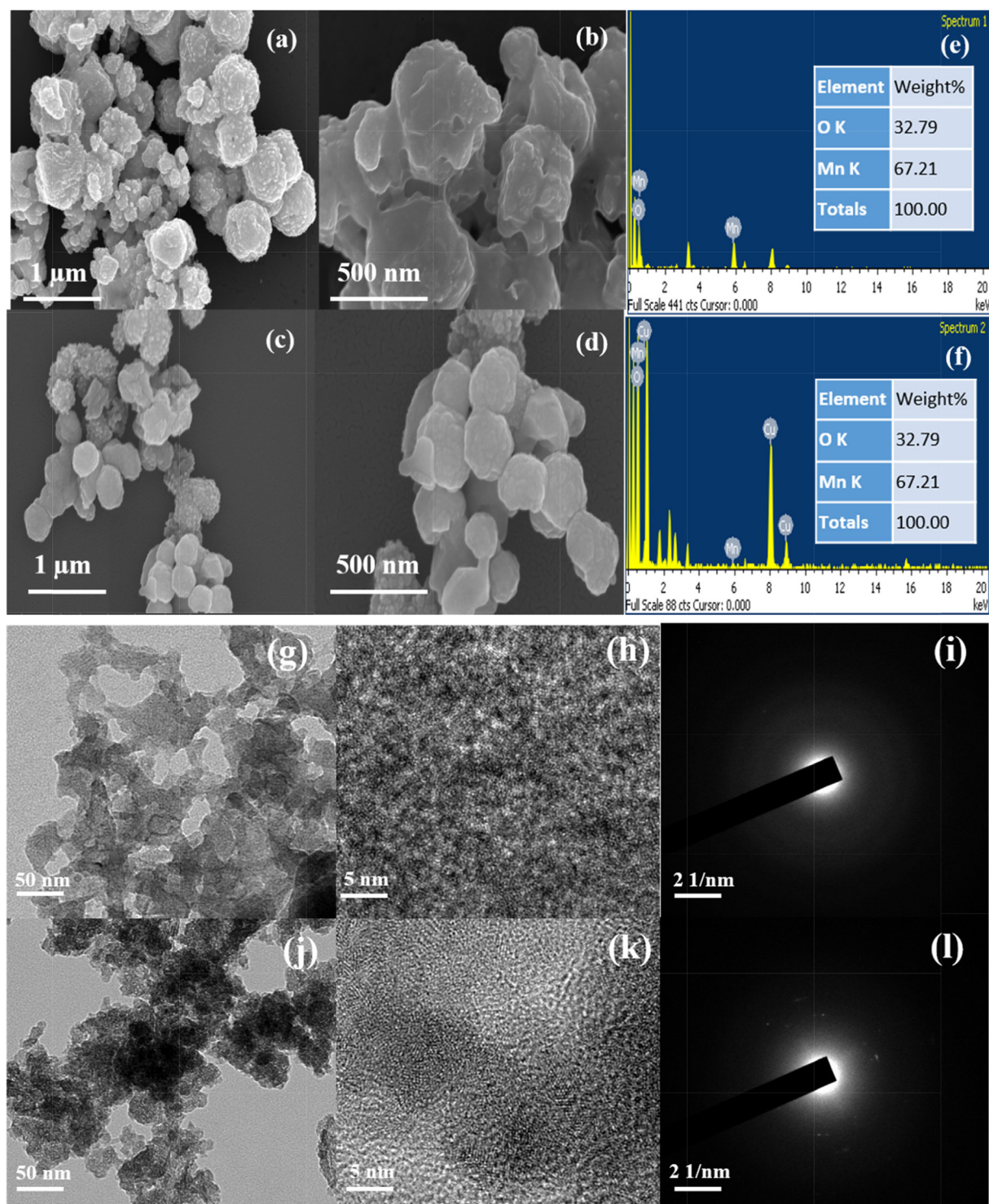


Fig. 3 FE-SEM micrographs of (a-b) MnO₂, (c-d) 10 wt% Cu- MnO₂ and (e,f) EDS images of MnO₂ and 10 wt% Cu- MnO₂ nanoparticles. TEM micrographs of (g,h) MnO₂, (j,k) 10 wt% Cu- MnO₂ and (i,l) SAED images of MnO₂ and 10 wt% Cu- MnO₂ nanoparticles.

using two identical electrodes coated with Pt and Cu doped MnO₂ samples by plotting logarithmic current density as a function of voltage. The higher exchange current density (J_0) has been observed (Fig. 7, Table 1) for the Pt CE (1.17 mAcm^{-2}) which is well supported by the lower R_{CT} value compared to that of the 10 wt% Cu doped MnO₂ CE

(0.055 mAcm^{-2}) indicating better electrocatalysts for good reaction kinetics.

The fabricated solar cells of type FTO/TiO₂/N3dye/liquid electrolyte/copper doped MnO₂/FTO were analyzed under **0.85 Sun** (85 mW cm^{-2} , AM 1.5 G solar simulator; Refer to [supporting information](#) for experimental procedure toward

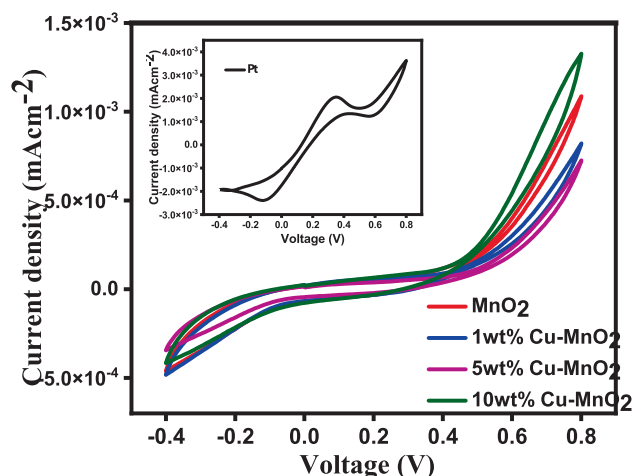


Fig. 4 CV curves of MnO₂ and 1, 5, & 10 wt% Cu doped MnO₂ Nanoparticles. (Inset shows CV for Pt electrode for comparison).

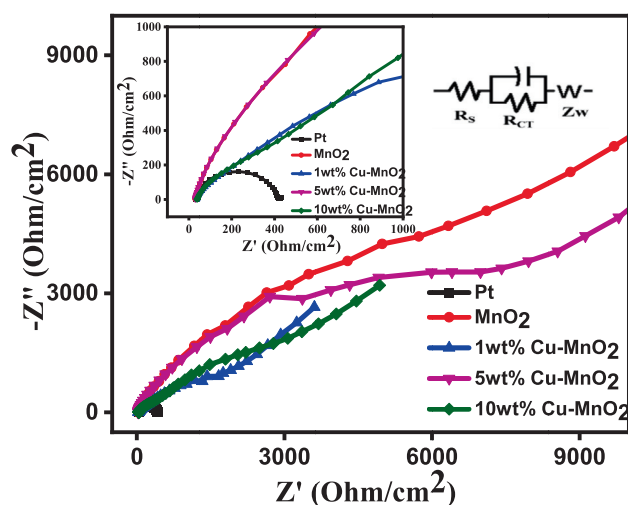


Fig. 5 Nyquist plots of symmetrical dummy cells fabricated with Pt, MnO₂, 1 wt% Cu-MnO₂, 5 wt% Cu-MnO₂, and 10 wt% Cu-MnO₂ CEs. Inset see equivalent circuit of CEs.

Table 1 EIS and Tafel parameters of prepared electrodes.

Electrodes	R _S (Ω cm ²)	R _{CT} (Ω cm ²)	J ₀ (mA cm ⁻²)
Pt	31.97	191.53	1.17
MnO ₂	30.29	164.70	0.0089
1 wt% Cu- MnO ₂	38.62	157.95	0.0079
5 wt% Cu- MnO ₂	29.87	278.46	0.0067
10 wt% Cu- MnO ₂	35.55	204.90	0.0055

the fabrication of solar cells). The open-circuit voltage (V_{oc}), short-circuit current (I_{sc}), fill factor (FF), and PCE (η) was calculated from the measured J-V curves (Fig. 8) using the AUTOLAB12/FRA2 PGSTAT302N model.

The device fabricated with pristine MnO₂ CE showed V_{oc} of 724 mV, I_{sc} of 2.71 mA/cm², FF of 0.53, and a power conversion efficiency of 1.21%. 1 wt% Cu doped MnO₂ showed enhanced % PCE of 1.4 compared with MnO₂ CE with V_{oc}

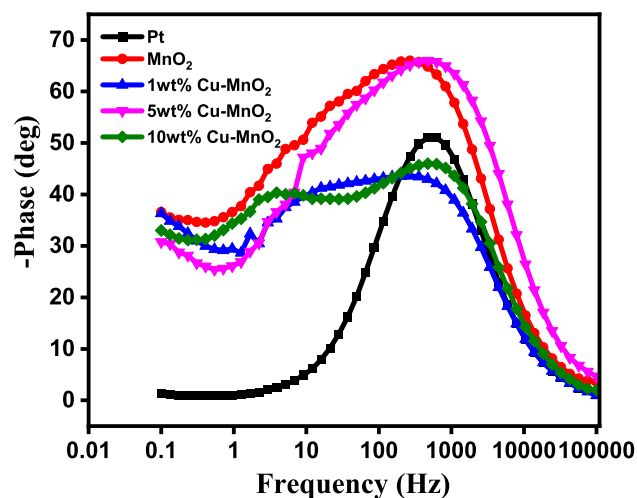


Fig. 6 Bode phase plots of dummy cells fabricated with Pt, MnO₂, 1 wt% Cu-MnO₂, 5 wt% Cu-MnO₂, and 10 wt% Cu-MnO₂ CEs.

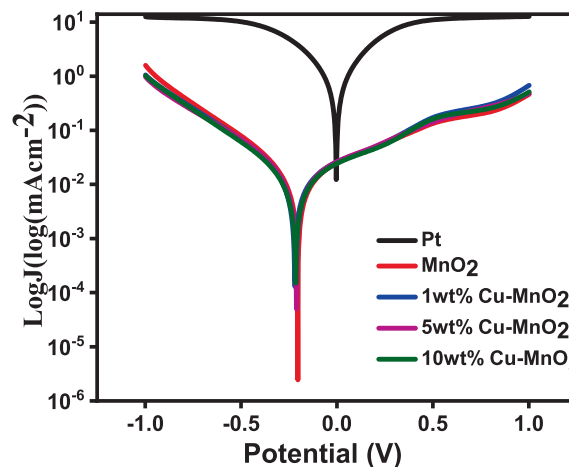


Fig. 7 Comparison of Tafel polarization curve of Pt with respect to MnO₂, 1 wt% Cu-MnO₂, 5 wt% Cu-MnO₂, and 10 wt% Cu-MnO₂ CEs.

of 726 mV, I_{sc} of 3.05 mA/cm² and improved FF of 0.54. 5 wt% Cu doped MnO₂ CE showed V_{oc} of 754 mV, I_{sc} of 3.17 mA/cm², FF of 0.52, and % PCE of 1.47. 10 wt% Cu doped MnO₂ CE showed the best V_{oc} of 781 mV, I_{sc} of 3.69 mA/cm², FF of 0.50, and % PCE of 1.7. The DSSC fabricated with Pt CE showed V_{oc} of 780 mV, I_{sc} of 6.8 mA/cm², FF of 0.43, and % PCE of 5.83. These results highlight that Cu doped MnO₂ is far better catalytic activity compared to pristine MnO₂. (Table 2).

The Nyquist plots of fabricated DSSCs with Pt, MnO₂, 1 wt% Cu-MnO₂, 5 wt% Cu-MnO₂, and 10 wt% Cu-MnO₂ CEs were shown in Fig. 9(A) (Table 2). The doped samples were found to have lower R_{CT} than pure MnO₂ samples indicating that the resistance for charge transfer got reduced. A lower R_{CT} value illustrates less overpotential is required for the electron transport between the electrolyte and CE indicating a higher tri-iodide reduction (I/I_3) and hence high fill factor.

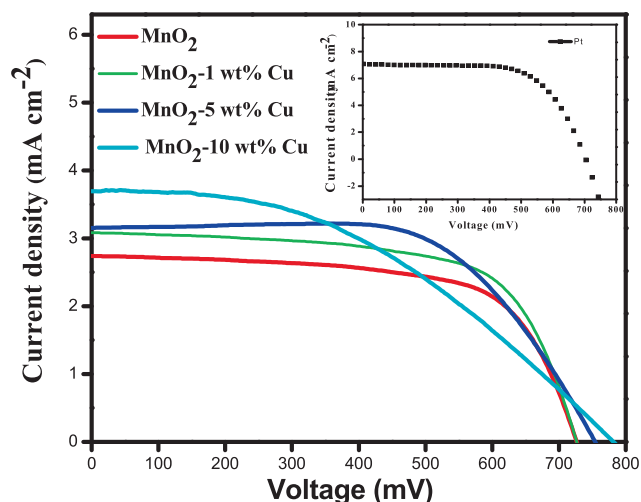


Fig. 8 I-V characteristics of DSSCs fabricated with Pt, MnO₂, 1 wt% Cu-MnO₂, 5 wt% Cu-MnO₂, and 10 wt% Cu-MnO₂ CEs.

In DSSCs, after electron injection from dye molecule into TiO₂, there is three possible recombination reactions with the electron acceptors viz. oxidized dye molecule, oxidized electrolyte species, and electron scavenger contaminants in the system. But the recombination reaction of the electron with the oxidized dye molecule is often least considered because this recombination is found to be slower (in the range of 10⁻⁴ s)

than the regeneration of the dye molecule (10⁻⁶ s) by the iodide ion [Bisquert et al. (2004)]. Hence, the primary recombination reaction is between TiO₂ and the oxidized ions in the electrolyte solution. Here, the electron lifetime is calculated using the formula $\tau = 1/2\pi f$, where the frequency is obtained from the Bode plot under illumination conditions at open circuit voltage. The Bode phase plot of the fabricated DSSCs with Pt, MnO₂, 1 wt% Cu-MnO₂, 5 wt% Cu-MnO₂, and 10 wt% Cu-MnO₂ CEs was shown in Fig. 9(B). From the Bode phase plot, the electron lifetime can be calculated which illustrates Cu doped MnO₂ samples are better than pristine MnO₂ (Table 2). The device fabricated with Pt CE showed the lower electron lifetime (0.18 ms) compared to 10 wt% Cu doped MnO₂ CE (0.79 ms) suggests decreased electron transfer at TiO₂ layer makes Pt CE less efficient for dye regeneration. While, the longer electron lifetime of Cu doped MnO₂ CE strongly supports the efficient dye regeneration due to fast electron transfer evidencing the superior electrocatalytic activity. The device fabricated with Pt CE showed the lowest R_{CT} value of 96.02 Ω cm⁻² suggesting the fast electron transfer process at CE/electrolyte interface.

Further, a comparable table reflection the improvement with a novel CE are presented in Table 3 illustrate that the initial results of copper doped MnO₂ are found satisfactory. This is because in the case of copper doped MnO₂, the added copper ion leads to increase the amount of Mn³⁺ at the surface and in turn improves the catalytic activity. Besides, added copper dopant increased the covalent nature of Mn-O bonds and results in stabilization and faster kinetics rate of electrode.

Table 2 Current-Voltage, EIS and life-time parameters of DSSCs fabricated with Pt, MnO₂, 1 wt% Cu-MnO₂, 5 wt% Cu-MnO₂, and 10 wt% Cu-MnO₂ CEs.

CE	V _{OC} (mV)	I _{SC} (mA/cm ²)	FF	PCE%	R _s (Ω cm ²)	R _{CT} (Ω cm ²)	τ ₁ (ms)
Pt	780	14.8	0.43	5.83	56.13	96.02	0.18
MnO ₂	724	2.71	0.53	1.21	35.07	184.34	0.79
1 wt% Cu- MnO ₂	726	3.05	0.54	1.40	21.52	102.26	1.04
5 wt% Cu- MnO ₂	754	3.17	0.52	1.47	21.14	131.26	0.59
10 wt% Cu- MnO ₂	781	3.69	0.50	1.70	20.31	108.97	0.79

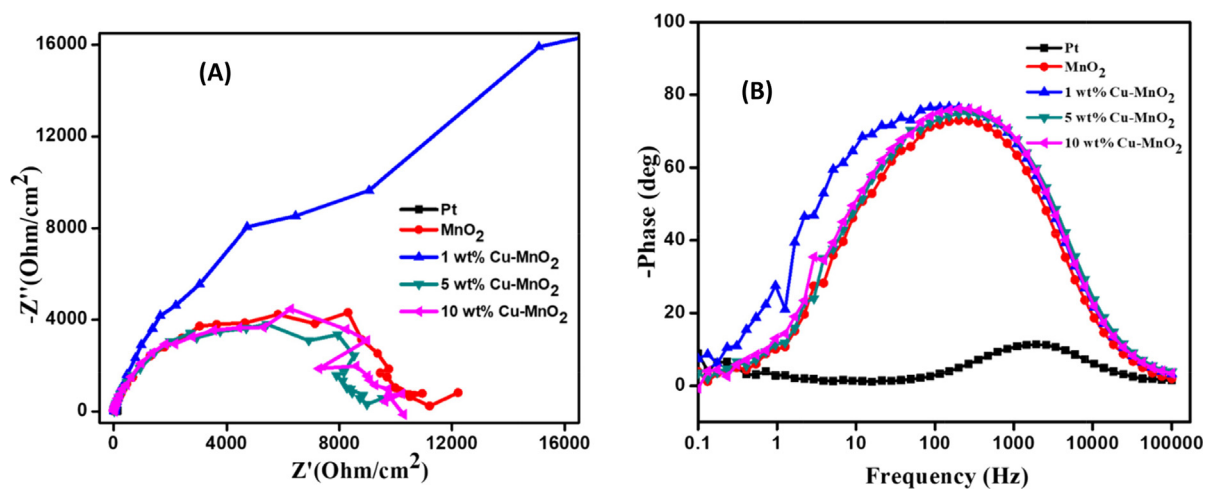


Fig. 9 Nyquist (A) and Bode phase (B) plots (under dark) of DSSCs fabricated with Pt, MnO₂, 1 wt% Cu-MnO₂, 5 wt% Cu-MnO₂, and 10 wt% Cu-MnO₂ CEs.

Table 3 Comparison of research progress of fabricated DSSCs with different CEs.

CE	V _{OC} (mV)	I _{SC} (mA/cm ²)	FF	PCE%	Ref
10 wt% Cu- MnO ₂	781	3.69	0.50	1.70	This work
α-MnO ₂ nanorods	750	14.7	0.38	4.1	Ahmad et al. 2017
MnO ₂ -carbon nanofiber composite	783	16.15	0.70	8.86	Li et al. 2017
MnO ₂ -NiO composite	830	0.3	0.84	0.21	Kakroo et al. 2020
Fe ₃ C-1 %Cu	700	12.72	0.61	5.46	Cai et al. 2017
Cu:TiO ₂ /TiO ₂	1073	7.52	0.55	4.87	Ünlü and Özacar 2020

All these factors may be responsible for the improvement of efficiency upon compared to pristine MnO₂.

4. Conclusions

MnO₂ and copper doped MnO₂ nanoparticles have been successfully produced by the hydrothermal method. The formation of the tetragonal crystal structure of α-MnO₂ and its copper doped versions was established by XRD analysis. The electrochemical characterization of MnO₂ and copper doped MnO₂ nanoparticles show the electrocatalytic property of the respective electrodes toward the reduction of I₃⁻ ions. Even though the samples do not show the distinct oxidation and reduction peaks in the CV study, the DSSC devices fabricated with MnO₂ and copper doped MnO₂ CEs behave like diodes under dark (no light is present). Among the fabricated DSSCs 10 wt% Cu doped MnO₂ cathodes yield the highest energy conversion efficiency of 1.7% than the pristine MnO₂ which had only 1.21% PCE. Further study regarding the choice of a material having electrocatalytic activity as good as Pt may lead to the fabrication of low-cost Pt-free DSSCs.

Declaration of Competing Interest

The authors declare that they have no known competing financial interests or personal relationships that could have appeared to influence the work reported in this paper.

Acknowledgments

The authors are thankful to the Deanship of Scientific Research at Najran University for funding this work under the National Research Priorities funding program (NU/NRP/SERC/11/9).

Appendix A. Supplementary material

Supplementary data to this article can be found online at <https://doi.org/10.1016/j.arabjc.2022.104068>.

References

Ahmad, K., Mohammad, A., Mobin, S.M., 2017. Hydrothermally grown α-MnO₂ nanorods as highly efficient low-cost counter-electrode material for dye-sensitized solar cells and electrochemical sensing applications. *Electrochim. Acta* 252, 549–557.

An, D., Zhang, Y., Zhang, H., Ma, G., Zhang, C., Ma, Z., 2019. Synthesis of copper-doped MnO₂ electrode materials by one-step hydrothermal method for high performance. *Acta Chim. Slov.* 66, 584–591.

Atilgan, A., Yildiz, A., 2022. Ni-doped TiO₂/TiO₂ homojunction photoanodes for efficient dye-sensitized solar cells. *Int. J. Energy Res.* <https://doi.org/10.1002/er.8175>. In press.

Atli, A., Yildiz, A., 2022. Opaque Pt counter electrodes for dye-sensitized solar cells. *Int. J. Energy Res.* 46, 6543–6552.

Bisquert, J., Cahen, D., Hodes, G., Rühle, S., Zaban, A., 2004. Physical Chemical Principles of Photovoltaic Conversion with Nanoparticulate, Mesoporous Dye-Sensitized Solar Cells. *J. Phys. Chem. B*, 108, 8106–8118.

Cai, H., Li, J., Want, R., Wu, F., Tong, X., 2017. Copper-doped Iron carbide as counter electrodes for dye-sensitized solar cells. *Int. J. Electrochem. Sci.* 12, 8421–8431.

Chiba, Y., Islam, A., Watanabe, Y., Komiya, R., Koide, N., Han, L., 2006. Dye-sensitized solar cells with a conversion efficiency of 11.1%. *Jpn. J. Appl. Phys.* 45, 638–640.

Datta, S., Dey, A., Ranjan Singha, N., Roy, S., 2020. Enhanced performance of dye-sensitized solar cell with thermally stable natural dye-assisted TiO₂/MnO₂ bilayer-assembled photoanode. *Mat. Renew. Sus. Energy* 9, 25–1–25–11.

Davis, D.J., Lambert, T.N., Vigil, J.A., Rodriguez, M.A., Brumbach, M.T., Coker, E.N., Limmer, S.J., 2014. Role of Cu-ion doping in Cu-α-MnO₂ nanowire electrocatalysts for the oxygen reduction reaction. *J. Phy. Chem. C* 118, 17342–17350.

Ding, K.-Q., 2010. Cyclic voltammetrically prepared copper-decorated MnO₂ and its electrocatalysis for oxygen reduction reaction (ORR). *Int. J. Electrochem. Sci.* 5, 72–87.

Furimsky, E., 2003. Metal carbides and nitrides as potential catalysts for hydroprocessing. *Appl. Catal.* 40, 1–28.

Gao, C., Han, Q., Wu, M., 2018. Review on transition metal compounds-based counter electrode for dye-sensitized solar cells. *J. Energy Chem.* 27, 703–712.

Huang, K.C., Hu, C.W., Tseng, C.Y., Liu, C.Y., Yeh, M.H., Wei, H. Y., Wang, C.C., Vittal, R., Chu, C.W., Ho, K.C., 2012. A counter electrode based on hollow spherical particles of polyaniline for a dye-sensitized solar cell. *J. Mater. Chem.* 22, 14727–14733.

Jeon, S.S., Kim, C., Ko, J., Im, S.S., 2011. Spherical polypyrrole nanoparticles as a highly efficient counter electrode for dye-sensitized solar cells. *J. Mater. Chem.* 21, 8146–8151.

Jiang, Q.W., Li, G.R., Gao, X.P., 2009. Highly ordered TiN nanotube arrays as counter electrodes for dye-sensitized solar cells. *Chem. Commun.* 44, 6720–6722.

Julien, C.M., Mauger, A., 2017. Nanostructured MnO₂ as electrode materials for energy storage. *Nanomaterials* 7, 396.

Kakroo, S., Surana, K., Bhattacharya, B., 2020. Electrodeposited MnO₂-NiO composites as a Pt free counter electrode for dye-sensitized solar cells. *J. Electro. Mater.* 49, 2197–2202.

Kang, J.S., Park, M.A., Kim, J.Y., Park, S.H., Chung, D.Y., Yu, S.H., Kim, J., Park, J., Choi, J.W., Lee, K.J., Jeong, J., Ko, M.J., Ahn, K.S., Sung, Y.E., 2015. Reactively sputtered nickel nitride as electrocatalytic counter electrode for dye- and quantum dot-sensitized solar cells, sensitizers, electrolytes, and counter electrodes. *Sci. Rep.* 5 (10450). <https://doi.org/10.1038/srep10450>.

Kim, H., Choi, H., Hwang, S., Kim, Y., Jeon, M., 2012. Fabrication and characterization of carbon-based counter electrodes prepared by electrophoretic deposition for dye-sensitized solar cells. *Nanoscale Res. Lett.* 7, 53.

Kim, J.Y., Lee, K.J., Kang, S.H., Shin, J., Sung, Y.E., 2011. Enhanced photovoltaic properties of a cobalt bipyridyl redox electrolyte in

- dye-sensitized solar cells employing vertically aligned TiO₂ nanotube electrodes. *J. Phys. Chem. C* 115, 19979–19985.
- Kim, S.S., Nah, Y.C., Noh, Y.Y., Jo, J., Kim, D.Y., 2006. Electrodeposited Pt for cost-efficient and flexible dye-sensitized solar cells. *Electrochim. Acta* 51, 3814–3819.
- Kiran, R., Leev, P., Aleksandra, A.-R., Kirill, A., Valerii, L., Elena, S., 2016. An introduction to solar cell technology. *J. Appl. Eng. Sci.* 14, 481–491.
- Li, L., Lu, Q., Xiao, J., Li, J., Mi, H., Duan, R., Li, J., Zhang, W., Li, X., Liu, S., Yang, K., Wu, M., Zhang, Y., 2017. Synthesis of highly effective MnO₂ coated carbon nanofibers composites as low cost counter electrode for efficient dye-sensitized solar cells. *J. Power Sources* 363, 9–15.
- Li, Q., Yin, L., Li, Z., Wang, X., Qi, Y., Ma, J., 2013. Copper doped hollow structured manganese oxide mesocrystals with controlled phase structure and morphology as anode materials for lithium ion battery with improved electrochemical performance. *ACS Appl. Mater. Interfaces* 5, 10975–10984.
- Lin, X., Wu, M., Wang, Y., Hagfeldt, A., Ma, T., 2011. Novel counter electrode catalysts of niobium oxides supersede Pt for dye-sensitized solar cells. *Chem. Commun.* 47, 11489–11491.
- Luo, J., Zhu, H.T., Fan, H.M., Liang, J.K., Shi, H.L., Rao, G.H., Li, J.B., Du, Z.M., Shen, Z.X., 2008. Synthesis of single-crystal tetragonal α -MnO₂ nanotubes. *J. Phys. Chem. C* 112, 12594–12898.
- Mondal, D., Paul, B.K., Das, S., Bhattacharya, D., Ghoshal, D., Nandy, P., Das, K., Das, S., 2018. Synthesis and property of copper-impregnated α -MnO₂ semiconductor quantum dots. *Langmuir* 34, 12702–12712.
- Mondal, D., Das, S., Paul, B.K., Bhattacharya, D., Ghoshal, D., Gayen, A.L., Das, K., Das, S., 2019. Size engineered Cu-doped α -MnO₂ nanoparticles for exaggerated photocatalytic activity and energy storage application. *Mat. Res. Bull.* 115, 159–169.
- Murakami, T.N., Gratzel, M., 2008. Counter electrodes for DSC: application of functional materials as catalysts. *Inorg. Chim. Acta* 361, 572–580.
- Nam, J.G., Park, Y.J., Kim, B.S., Lee, J.S., 2010. Enhancement of the efficiency of dye-sensitized solar cell by utilizing carbon nanotube counter electrode. *Scr. Mater.* 62, 148–150.
- Olsen, E., Hagen, G., Lindquist, S.E., 2000. Dissolution of platinum in methoxy propionitrile containing LiI/I₂. *Sol. Energy Mater. Sol. Cells* 63, 267–273.
- Paranthaman, V., Muthu, S., Alagarsamy, P., Ming, H., Perumalsamy, R., 2016. Influence of zirconium dioxide and titanium dioxide binders on the photovoltaic performance of dye sensitized solar cell tungsten carbide nanorods based counter electrode. *Electrochim. Acta* 211, 375–384.
- Sarker, S., Ahammad, A. J. S., Seo, H. W., Kim D. M., 2014. Electrochemical Impedance Spectra of Dye-Sensitized solar cells: Fundamentals and Spreadsheet Calculation. *Int. J. Photoenergy* 2014, 851705 (1-17).
- Thomas, S., Deepak, T.G., Anjusree, G.S., Arun, T.A., Nair, S.V., Sreekumaran Nair, A., 2014. A review on counter electrode materials in dye-sensitized solar cells. *J. Mater. Chem. A* 2, 4474–4490.
- Ünlü, B., Özacar, M., 2020. Effect of Cu and Mn amounts doped to TiO₂ on the performance of DSSCs. *Sol Energy* 196, 448–456.
- Vijaya, S., Landi, G., Wu, J.J., Ashokkumar, M., Anandan, S., 2021. Platinum-free dye-sensitized solar cells by flower-like mixed-phase CoxSy/NixSy/MoxSy composites. *New J. Chem.* 45, 1967–1976.
- Vijayakumar, P., Pandian, M.S., Lim, S.P., Pandikumar, A., Huang, N.M., Mukhopadhyay, S., Ramasamy, P., 2015. Facile synthesis of tungsten carbide nanorods and its application as counter electrode in dye-sensitized solar cells. *Mat. Sci. in Semicon. Proc.* 39, 292–299.
- Wang, L., Al-Mamun, M., Liu, P., Wang, Y., Yang, H.G., Wang, H. F., Zhao, H., 2015. The search for efficient electrocatalysts as counter electrode materials for dye-sensitized solar cells: mechanistic study, material screening and experimental validation. *NPG Asia Mater.* 7, e226.
- Wei, W., Cui, X., Chen, W., Ivey, D.G., 2011. Manganese oxide-based materials as electrochemical supercapacitor electrodes. *Chem. Soc. Rev.* 40, 1697–1721.
- Wu, J., Lan, Z., Lin, J., Huang, M., Huang, Y., Fan, L., Luo, G., Lin, Y., Xie, Y., Wei, Y., 2017. Counter electrodes in dye-sensitized solar cells. *Chem. Soc. Rev.*, 46, 5975.
- Wu, M., Lin, X., Wang, Y., Wang, L., Guo, W., Qu, D., Peng, X., Hagfeldt, A., Gratzel, M., Ma, T., 2012. Economical Pt-free catalysts for counter electrodes of dye-sensitized solar cells. *J. Am. Chem. Soc.* 134, 3419–3428.
- Wu, M., Wang, Y., Lin, X., Yu, N., Wang, L., Wang, L., Hagfeldt, A., Ma, T., 2011. Economical and effective sulfide catalysts for dye-sensitized solar cells as counter electrodes. *Phys. Chem. Chem. Phys.* 13, 19298–19301.
- Yang, Y., Huang, X., Yang, Y., Wu, C., Lei, B., Peng, Q., Wang, G., 2019. Improving the rate performance of manganese dioxide by doping with Cu²⁺, Co²⁺ and Ni²⁺ ions. *Int. J. Electrochem. Sci.* 14, 3673–3683.
- Yildiz, A., Chouki, T., Atli, A., Harb, M., Verbruggen, S.W., Ninakanti, R., Emin, S., 2021. Efficient iron phosphide catalyst as a counter electrode in dye-sensitized solar cells. *ACS Appl. Energy Mater.* 4, 10618–10626.
- Yun, S., Wang, L., Zhao, C., Wang, Y., Ma, T., 2013. A new type of low-cost counter electrode catalyst based on platinum nanoparticles loaded onto silicon carbide (Pt/SiC) for dye-sensitized solar cells. *Phys. Chem. Chem. Phys.* 15, 4286–4290.
- Zhang, X., Chen, X., Dong, S., Liu, Z., Zhou, X., Yao, J., Pang, S., Xu, H., Zhang, Z., Lia, L., Cui, G., 2012. Hierarchical micro/nano-structured titanium nitride spheres as a high-performance counter electrode for a dye-sensitized solar cell Hierarchical micro/nano-structured titanium nitride spheres as a high-performance counter electrode for a dye-sensitized solar cell. *J. Mater. Chem. A* 22, 6067–6071.
- Zhou, H., Shi, Y., Wang, L., Zhang, H., Zhao, C., Hagfeldt, A., Ma, T., 2013. Notable catalytic activity of oxygen-vacancy-rich WO_{2.72} nanorod bundles as counter electrodes for dye-sensitized solar cells. *Chem. Commun.* 49, 7626–7628.
- Zulkifli, A.N.B., Kento, T., Daiki, M., Fujiki, A., 2015. The basic research on the dye-sensitized solar cells. *J. Clean Energy Technol.* 3, 382–387.